Journal of Sound and Vibration (2002) **250**(5), 795–811
doi:10.1006/jsvi.2001.3951, available online at http://www.idealibrary.com on IDEAL®

VIBRATION AND STABILITY OF ROTATING POLAR ORTHOTROPIC ANNULAR DISKS SUBJECTED TO A STATIONARY CONCENTRATED TRANSVERSE LOAD

D.-S. Liang, H.-J. Wang and L.-W. Chen

Department of Mechanical Engineering, National Cheng Kung University, Tainan 70101, *Taiwan, Republic of China. E-mail: chenlw@mail.ncku.edu.tw*

(*Received* 15 *January* 2001, *and in final form* 21 *June* 2001)

In the present paper, natural frequencies and stability of a spinning polar orthotropic disk subjected to a stationary concentrated transverse load are investigated. The analysis of the free vibration of a spinning disk is performed first to find natural frequencies and corresponding vibration modes. The resulting eigenfunctions obtained from the free vibration are used as deflection functions of the forced vibration of a disk where the load is modelled as a mass–spring–dashpot system fixed in space. By using the Galerkin approximation method, eigenvalues of the whole system are determined. Results show that disks with higher values of modulus ratios or the Poisson ratios have higher natural frequencies, and the stability of the whole system can be improved by raising the value of the modulus ratio or lowering that of the Poisson ratio.

1. INTRODUCTION

The dynamics of spinning disks has been an interesting research topic because of its important applications in such fields as computer disk memory units, circular saws, and turbine rotors. The vibration responses of a rotating disk subjected to an external transverse force are mainly considered. It has been found that such a system becomes unstable at certain speeds of rotation, which depend only upon natural frequencies of the vibration of the disk. Such a phenomenon might reduce the performance of rotating machines. There is an increasing use of fibre-reinforced composite materials in the design and fabrication of mechanical components. The studies of the dynamic responses and stability problems of anisotropic plates are important and interesting topics.

Early investigations dealt with homogeneous isotropic spinning disks. Natural frequencies of the vibration and effects of various parameters in the load system on the stability were studied. Eversman and Dodson [1] examined the free vibration of a centrally clamped spinning disk and solutions are obtained by expansion in power series. Later, Barasch and Chen [2] repeated the same work, but determined natural frequencies by using the modified Adam's method. Iwan and Moeller [3] considered the stability of a spinning elastic disk with a transverse load system. They used the eigenfunction expansion method to calculate eigenvalues of the rotating disk system, and discussed the instability due to effects of the transverse mass, damping, and stiffness in the load system. Ono *et al.* [4] extended Iwan and Moeller's work to include pitching parameters in the load system as well as the friction force between the spinning disk and the stationary load system. Chen and Bogy [5] presented a theoretical study of a general gyroscopic system and applied it to a spinning disk in contact with a stationary load system to predict effects of parameter changes on

0022-460X/02/100795 + 17 $35.00/0

eigenvalues of the system. They further analyzed the mathematical structure of modal interactions of the same system [6].

As for anisotropic disks, Minkarah and Hoppmann [7] studied free vibrations of a stationary polar orthotropic disk, but only axis-symmetrical vibration modes were treated. Ginesu *et al.* [8] used the finite element method to analyze a similar problem. Narita [9] used the Rayleigh–Ritz method to analyze free vibrations of completely free annular and circular plates having polar orthotropy. Mbakogu and Pavlovic [10] dealt with closed-form fundamental-frequency estimates for polar orthotropic circular plates by means of Rayleigh's method. Asymmetric vibrations and elastic stability of polar orthotropic circular plates of variable thickness are presented by Gupta and Ansari [11, 12]. The vibrations of a circular plate with elastically restrained edge are considered. Recently, Pistonesi and Laura [13] investigated forced vibrations of the clamped rectangular orthotropic circular plate subjected to a harmonic excitation. Furthermore, Gutiérrez and Laura [14] also dealt with the transverse vibration of polar orthotropic circular plates with a concentric circular support.

To the authors' knowledge, no work has been done to study the vibration and stability of a spinning polar orthotropic disk with a concentrated transverse load system. In the present paper, the free vibration of spinning polar orthotropic disks is performed first to obtain natural frequencies and corresponding vibration modes. The deflections of the forced vibration of the disk are expressed in terms of the eigenfunctions obtained from the free vibration. Then, the forced vibration problems of a disk subjected to a concentrated load modelled as a mass–spring–dashpot system are solved.

2. BASIC EQUATION

A homogenous, polar orthotropic, thin annular disk of uniform thickness subjected to a transverse load distribution $q(r, \theta, t)$ is shown in Figure 1. The disk is rigidly clamped at inner radius $r = a$, free at outer radius $r = b$ and spins about z-axis at a constant angular speed Ω. Under assumptions of the classical plate theory, the in-plane membrane forces of rotation are assumed to be unaffected by the transverse motion of the disk, and effects of the gravity and in-plane vibrations are also neglected. The governing partial differential equation of the transverse motion for the disk in co-ordinates (r, θ, z) moving with the disk may be written in the form [15, 16]

$$D_r \frac{\partial^4 w}{\partial r^4} + 2D_{r\theta} \frac{1}{r^2} \frac{\partial^4 w}{\partial r^2 \partial \theta^2} + D_\theta \frac{1}{r^4} \frac{\partial^4 w}{\partial \theta^4} + 2D_r \frac{1}{r} \frac{\partial^3 w}{\partial r^3} - 2D_{r\theta} \frac{1}{r^3} \frac{\partial^4 w}{\partial r \partial \theta^2}$$

$$- D_\theta \frac{1}{r^2} \frac{\partial^2 w}{\partial r^2} + 2(D_{r\theta} + D_\theta) \frac{1}{r^4} \frac{\partial^2 w}{\partial \theta^2} + D_\theta \frac{1}{r^3} \frac{\partial w}{\partial r} - \frac{h}{r} \left[\frac{\partial}{\partial r} \left(r\sigma_r^0 \frac{\partial w}{\partial r} \right) \right.$$

$$\left. + \frac{\partial}{\partial \theta} \left(\frac{\sigma_\theta^0}{r} \frac{\partial w}{\partial \theta} \right) \right] + \rho h \frac{\partial^2 w}{\partial t^2} = q(r, \theta, t), \tag{1}$$

where $w = w(r, \theta, t)$ is the transverse displacement of the point (r, θ) on the disk at time t; the D's are flexural and twisting rigidities defined as $D_r = E_r h^3/12(1 - v_r v_\theta)$, $D_\theta = E_\theta h^3/12(1 - v_r v_\theta)$, $D_k = G_{r\theta} h^3/12$, and $D_{r\theta} = v_\theta D_r + 2D_k$ with E_r, E_θ, and $G_{r\theta}$ being Young's moduli and shear modulus, respectively, h being the uniform thickness and v_r, v_θ being the Poisson ratios; ρ is the mass density; and σ_r^0 and σ_θ^0 are in-plane membrane

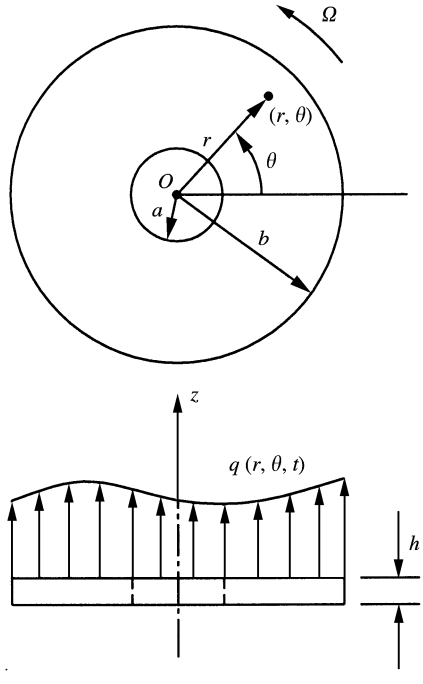

Figure 1. A spinning disk with a transverse distribution load.

stresses due to the centrifugal effect and are given by

$$\sigma_r^0(\bar{r}) = \frac{A}{B}\left[(k + v_\theta)C\bar{r}^{k-1} - (k - v_\theta)E\bar{r}^{-(k+1)} - (3 + v_\theta)B\bar{r}^2\right], \tag{2}$$

$$\sigma_\theta^0(\bar{r}) = \frac{A}{B}\left[k^2(v_r k + 1)C\bar{r}^{k-1} - k^2(v_r k - 1)E\bar{r}^{-(k+1)} - (3v_\theta + k^2)B\bar{r}^2\right] \tag{3}$$

with

$$A = \frac{\rho\Omega^2 b^2}{9 - k^2}, \qquad B = (k - v_\theta)\varsigma^{2k} + (k + v_\theta), \qquad C = (k - v_\theta)\varsigma^{k+3} + (3 + v_\theta),$$

$$E = (k + v_\theta)\varsigma^{k+3} - (3 + v_\theta)\varsigma^{2k}, \qquad \varsigma = \frac{a}{b}, \qquad \bar{r} = \frac{r}{b}, \qquad k = \sqrt{\frac{E_\theta}{E_r}}.$$

The boundary conditions for the clamped inner edge are

$$w|_{r=a} = 0, \quad \left.\frac{\partial w}{\partial r}\right|_{r=a} = 0, \tag{4, 5}$$

and at the free outer edge, we have

$$M_r|_{r=b} = 0, \qquad -Q_r + \frac{1}{r}\left.\frac{\partial M_{r\theta}}{\partial \theta}\right|_{r=b} = 0. \tag{6, 7}$$

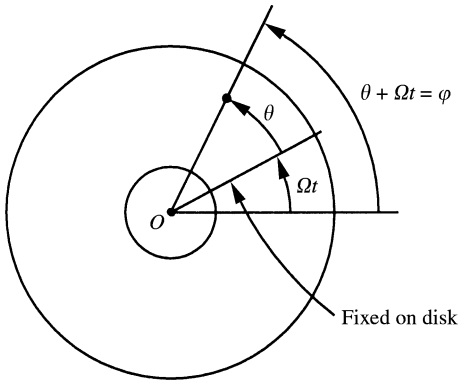

Figure 2. Relationship of space- and disk-fixed co-ordinates.

Equations (6) and (7) can further be written in terms of the transverse displacement w

$$D_r\left[\frac{\partial^2 w}{\partial r^2}+\nu_\theta\left(\frac{1}{r}\frac{\partial w}{\partial r}+\frac{1}{r^2}\frac{\partial^2 w}{\partial\theta^2}\right)\right]\Bigg|_{r=b}=0, \tag{8}$$

$$\left\{\left[D_r\left(\frac{\partial^3 w}{\partial r^3}+\frac{1}{r}\frac{\partial^2 w}{\partial r^2}\right)+D_{r\theta}\frac{1}{r^2}\frac{\partial^2}{\partial\theta^2}\left(\frac{\partial w}{\partial r}-\frac{w}{r}\right)-D_\theta\frac{1}{r^2}\left(\frac{\partial w}{\partial r}+\frac{1}{r}\frac{\partial^2 w}{\partial\theta^2}\right)\right]+\frac{2D_k}{r^2}\left(-\frac{1}{r}\frac{\partial^2 w}{\partial\theta^2}+\frac{\partial^3 w}{\partial r\partial\theta^2}\right)\right\}\Bigg|_{r=b}=0. \tag{9}$$

The equation of motion may also be referred to a reference frame fixed in space by means of the transformation

$$\varphi=\theta+\Omega t, \tag{10}$$

where φ is the absolute polar co-ordinate of a material point on the disk as indicated in Figure 2. The equation of motion becomes

$$D_r\frac{\partial^4 w}{\partial r^4}+2D_{r\theta}\frac{1}{r^2}\frac{\partial^4 w}{\partial r^2\partial\varphi^2}+D_\theta\frac{1}{r^4}\frac{\partial^4 w}{\partial\varphi^4}+2D_r\frac{1}{r}\frac{\partial^3 w}{\partial r^3}-2D_{r\theta}\frac{1}{r^3}\frac{\partial^3 w}{\partial r\partial\varphi^2}-D_\theta\frac{1}{r^2}\frac{\partial^2 w}{\partial r^2}+2(D_{r\theta}+D_\theta)\frac{1}{r^4}\frac{\partial^2 w}{\partial\varphi^2}+D_\theta\frac{1}{r^3}\frac{\partial w}{\partial r}-\frac{h}{r}\left[\frac{\partial}{\partial r}\left(r\sigma_r^0\frac{\partial w}{\partial r}\right)+\frac{\partial}{\partial\varphi}\left(\frac{\sigma_\theta^0}{r}\frac{\partial w}{\partial\varphi}\right)\right]+\rho h\left(\Omega^2\frac{\partial^2 w}{\partial^2\varphi}+2\Omega\frac{\partial^2 w}{\partial t\partial\varphi}+\frac{\partial^2 w}{\partial t^2}\right)=q(r,\varphi,t). \tag{11}$$

Since the boundary conditions are axisymmetric, equations (4), (5), (7) and (8) can also be applied.

3. FREE VIBRATION

Natural frequencies and mode shapes from a free vibration analysis will provide significant information for obtaining the response of a forced vibration system. The free vibration of the annular disk may be studied by letting $q(r,\theta,t)=0$ in equation (1); here, the response of the disk is considered in the plate-fixed co-ordinate (r,θ,t). Assume that

the deflection is $w = \phi(r, \theta)e^{i\omega t}$, where ω is the natural frequency of the disk and $\phi(r, \theta)$ is the corresponding vibrating mode which can be expanded by Fourier series as

$$\phi(r, \theta) = \sum_{n=0}^{\infty} Y_n(r) \cos n\theta. \tag{12}$$

Equation (1) then becomes an ordinary differential equation on $Y(r)$ as follows:

$$\left\{D_r \frac{d^4}{dr^4} + 2D_r \frac{1}{r}\frac{d^3}{dr^3} - \left(2D_{r\theta}\frac{n^2}{r^2} + D_\theta \frac{1}{r^2} + h\sigma_r^0\right)\frac{d^2}{dr^2} + \left(2D_{r\theta}\frac{n^2}{r^3} + \frac{D_\theta}{r^3} - \frac{h}{r}\sigma_r^0 - h\frac{d\sigma_r^0}{dr}\right)\frac{d}{dr}\right.$$
$$\left. + \left[D_\theta \frac{n^4}{r^4} - 2(D_\theta + D_{r\theta})\frac{n^2}{r^4} + h\sigma_\theta^0 \frac{n^2}{r^2}\right]\right\} Y_{mn}(r) \tag{13}$$
$$= \rho h \omega_{mn}^2 Y_{nm}(r) \quad (n = 0, 1, 2, \dots).$$

Here the index m has been introduced to represent the mth mode solution of equation (13).

To simplify the calculation and analysis, the following dimensionless parameters are introduced:

$$\varsigma = \frac{a}{b}, \qquad \bar{w} = \frac{w}{h}, \qquad \bar{Y}_{mn} = \frac{Y_{mn}(r)}{h}, \qquad \bar{r} = \frac{r}{b}, \quad \bar{t} = \frac{t}{t_0}, \qquad \bar{\Omega} = \Omega t_0,$$
$$\bar{\omega}_{mn} = \omega_{mn} t_0, \qquad t_0 = \left(\frac{\rho h b^4}{D_r}\right)^{1/2}, \qquad \bar{\sigma}_r^0 = \frac{\sigma_r^0}{\sigma_0}, \qquad \bar{\sigma}_\theta^0 = \frac{\sigma_\theta^0}{\sigma_0}, \qquad \sigma_0 = \frac{D_r}{bh^2}. \tag{14}$$

Then equation (13) can be rewritten as

$$\left\{\frac{d^4}{d\bar{r}^4} + \frac{2}{\bar{r}}\frac{d}{d\bar{r}^3} - \left(\frac{S}{\bar{r}^2} + \bar{\sigma}_r^0\right)\frac{d^2}{d\bar{r}^2} + \left[\frac{S}{\bar{r}^3} - \left(\frac{\bar{\sigma}_r^0}{\bar{r}} + \frac{d\bar{\sigma}_r^0}{d\bar{r}}\right)\right]\frac{d}{d\bar{r}} + \left[\frac{T}{\bar{r}^4} + \frac{n^2\bar{\sigma}_\theta^0}{\bar{r}^2}\right]\right\}\bar{Y}_{mn}(\bar{r})$$
$$= \bar{\omega}_{mn}^2 \bar{Y}_{mn}(\bar{r}) \quad (n = 0, 1, 2, \dots), \tag{15}$$

where

$$S = 2n^2(2\mu + \nu_\theta) + k^2, \qquad T = n^4 k^2 - 2n^2(k^2 + 2\mu + \nu_\theta),$$
$$\mu = \frac{D_k}{D_r}, \quad 2\mu + \nu_\theta = \frac{D_{r\theta}}{D_r}.$$

The corresponding dimensionless boundary conditions can be expressed as

$$\bar{Y}_n(\bar{r})|_{\bar{r}=\varsigma} = 0, \qquad \left.\frac{d\bar{Y}_n(\bar{r})}{d\bar{r}}\right|_{\bar{r}=\varsigma} = 0, \tag{16, 17}$$

$$\left.\frac{d^2\bar{Y}_n(\bar{r})}{d\bar{r}^2} + \nu_\theta\left[\frac{1}{\bar{r}}\frac{d\bar{Y}_n(\bar{r})}{d\bar{r}} - \frac{n^2}{r^2}Y_n(\bar{r})\right]\right|_{\bar{r}=1} = 0, \tag{18}$$

$$\left\{\frac{d^3\bar{Y}_n(\bar{r})}{d\bar{r}^3} + \frac{1}{\bar{r}}\frac{d^2\bar{Y}_n(\bar{r})}{d^2\bar{r}} - \frac{1}{\bar{r}^2}[(4\mu + \nu_\theta)n^2 + k^2]\frac{d\bar{Y}_n(\bar{r})}{d\bar{r}}\right.$$
$$\left. + \frac{1}{\bar{r}^3}[(4\mu + \nu_\theta + k^2)n^2]\bar{Y}_n(\bar{r})\right\}\Bigg|_{\bar{r}=1} = 0. \tag{19}$$

The variational form of differential equation (15) and corresponding boundary conditions (16)–(19) can be written as

$$\int_{\varsigma}^{1} [(a_0 V)'' \bar{Y}'' - (a_1 V)' \bar{Y}'' + a_2 \bar{Y}'' V + a_3 \bar{Y}' V + a_4 \bar{Y} V] \, \mathrm{d}\bar{r} = \int_{\varsigma}^{1} \bar{\omega}^2 \bar{Y} V \, \mathrm{d}\bar{r}$$
$$- a_0(1) V(1)[\alpha_2 \bar{Y}'(1) + \beta_2 \bar{Y}(1)] + [(a_0 V)'(1) - a_1(1) V(1)][\alpha_1 \bar{Y}'(1) + \beta_1 \bar{Y}(1)], \quad (20)$$

where $\bar{Y} = \bar{Y}_{mn}(\bar{r})$ and V are the trial function and the test function, respectively, and the other parameters are given as follows:

$$a_0 = 1, \quad a_1 = \frac{2}{\bar{r}}, \quad a_2 = -\left(\frac{S}{\bar{r}^2} + \bar{\sigma}_r^0\right), \quad a_3 = \left[\frac{S}{\bar{r}^3} - \left(\frac{\bar{\sigma}_r^0}{\bar{r}} + \frac{\mathrm{d}\bar{\sigma}_r^0}{\mathrm{d}\bar{r}}\right)\right],$$
$$a_4 = \left(\frac{T}{\bar{r}^4} + \frac{n^2 \bar{\sigma}_\theta^0}{\bar{r}^2}\right), \qquad \alpha_1 = -\nu_\theta, \quad \alpha_2 = [(4\mu + \nu_\theta) n^2 + k^2 + \nu_\theta],$$
$$\beta_1 = n^2 \nu_\theta, \quad \beta_2 = -n^2(4\mu + 2\nu_\theta + k^2), \qquad \bar{\omega} = \bar{\omega}_{mn}.$$

The cubic Hermitian element is adopted for the present finite element solutions. For each element e, the approximate trial function and the test function can be denoted as

$$\bar{Y}^e(\bar{r}) = \sum_{j=1}^{4} \bar{Y}_1^e \psi_i^e(\bar{r}), \qquad V^e(\bar{r}) = \sum_{i=1}^{4} V_1^e \psi_i^e(\bar{r}), \quad (21, 22)$$

where $\psi_j^e(\bar{r})$ ($j = 1, 2, 3, 4$) are shape functions of the element e. Shape functions of the element are given by

$$\hat{\psi}_1(\xi) = \tfrac{1}{4}(2 - 3\xi + \xi^3), \quad \hat{\psi}_2(\xi) = \tfrac{1}{4}(2 + 3\xi - \xi^3),$$
$$\hat{\psi}_3(\xi) = \tfrac{1}{4}(1 - \xi - \xi^2 + \xi^3), \quad \hat{\psi}_4(\xi) = \tfrac{1}{4}(-1 - \xi + \xi^2 + \xi^3).$$

Substituting equations (21) and (22) into equation (20), we can obtain

$$\tilde{K}_{ij}^e \bar{Y}_j^e = \bar{\omega}^2 \tilde{M}_{ij}^e + (\text{integration terms of the boundary}) \quad (i, j = 1, 2, 3, 4), \quad (23)$$

where

$$\tilde{K}_{ij}^e = \int_{\Omega_r} (a_0'' \psi_i^e \psi_j^{e''} + 2a_0' \psi_i^{e'} \psi_j^{e''} + a_0 \psi_i^{e''} \psi_j^{e''} - a_1 \psi_i^{e'} \psi_j^{e''}$$
$$- a_0' \psi_i^e \psi_j^{e''} + a_2 \psi_i^e \psi_j^{e''} + a_3 \psi_i^e \psi_j^{e'} + a_4 \psi_i^e \psi_j^e) \, \mathrm{d}\bar{r} \ (e = 1, 2, \ldots, N_e),$$
$$\tilde{M}_{ij}^e = \int_{\Omega_e} \psi_i^e \psi_j^e \, \mathrm{d}\bar{r} \ (e = 1, 2, \ldots, N_e),$$

N_e is the element number, and Ω_e is the definition domain for the element e. The local element equations can be assembled to give the global finite element equation.

$$K_{IJ} \bar{Y}_J = \bar{\omega}^2 M_{IJ} \bar{Y}_J, \quad (24)$$

where

$$K_{IJ} = \sum_{e=1}^{N_e} \tilde{K}_{ij}^e + (\text{integration terms of boundaries of the first and final elements})$$
$$(I, J = 1, 2, \ldots, N_e),$$
$$M_{IJ} = \sum_{e=1}^{N_e} \tilde{M}_{ij}^e \quad (I, J = 1, 2, \ldots, N_e).$$

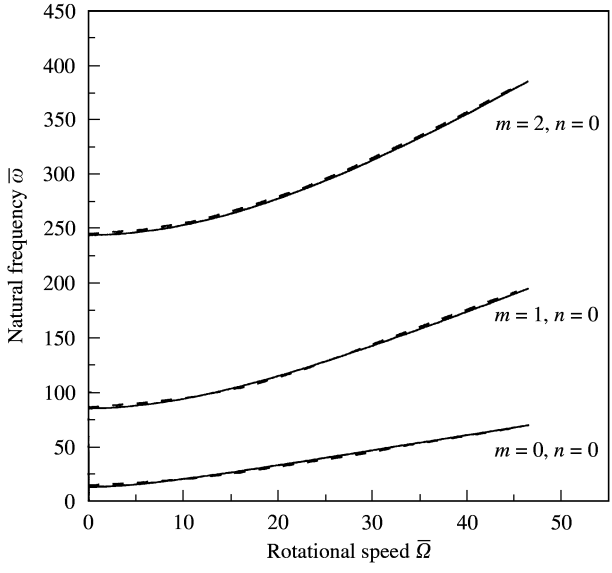

Figure 3. Effects of rotational speeds on natural frequencies ($E_\theta/E_r = 1{\cdot}0$. $a/b = 0{\cdot}5$ and $v_r = 0{\cdot}3$): – – –, Reference [2]; ——, proposed.

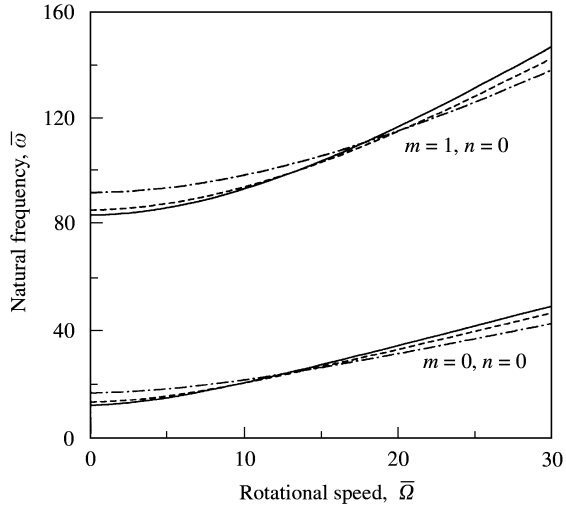

Figure 4. Effects of rotational speeds on natural frequencies for different modulus ratios $E_\theta/E_r = 0{\cdot}25$, $1{\cdot}0$ and $4{\cdot}0$ ($a/b = 0{\cdot}5$, $v_r = 0{\cdot}3$, $\mu = 0{\cdot}3$): ——, $E_\theta/E_r = 0{\cdot}25$; – – –, $E_\theta/E_r = 1{\cdot}0$; – · – · –, $E_\theta/E_r = 4{\cdot}0$.

Equation (24) forms an eigenvalue problem, which can be solved by using general numerical methods. Then, the dimensionless natural frequency $\bar{\omega}_{mn}$ and the dimensionless vibration mode shape in radius direction $\bar{Y}_{mn}(\bar{r})$ can be obtained.

Finite element solutions of the free vibration of a rotating polar orthotropic annular disk are presented in Figures 3–6. Ten elements are used in the present finite element calculations. The effects of the rotational speed on natural frequencies are shown in Figures 3 and 4. The isotropic case is considered in Figure 3, and the modulus ratio E_θ/E_r, the radial

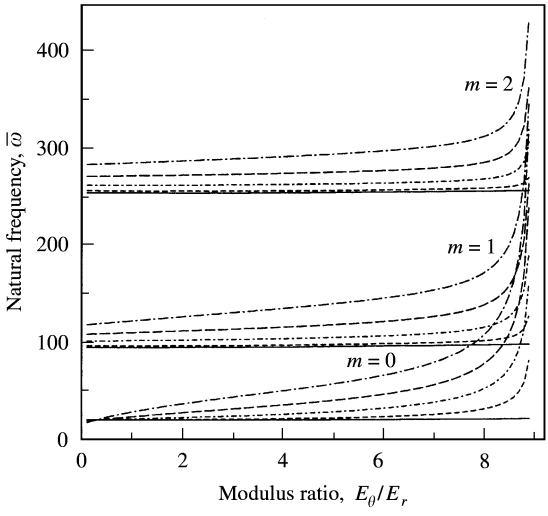

Figure 5. Effects of modulus ratios on natural frequencies ($a/b = 0{\cdot}5$, $\bar{\Omega} = 10$, $v_r = 0{\cdot}3$, $\mu = 0{\cdot}3$): ——, $n = 0$; - - - - -, $n = 1$; -·-·-·, $n = 2$; – – –, $n = 3$; –·–·–·, $n = 4$.

ratio ς and the Poisson ratio v_r are chosen to be 1·0, 0·5 and 0·3 respectively. It can be seen that the natural frequencies increase as the rotational speed increases and the results agree well with those obtained by Barasch and Chen [2]. The results of the circular orthotropic plate for different modulus ratios $E_\theta/E_r = 0{\cdot}25$, 1·0 and 4·0 are plotted in Figure 4. It can be seen that the plates with higher modulus ratio have higher natural frequency under lower rotational speed, but as the rotational speed increases above a certain number, the phenomenon is reversed. It also shows that effects of lower modulus ratios on natural frequencies are more sensitive as the rotational speed varies.

The effects of the modulus ratio on natural frequencies are shown in Figure 5 when the rotational speed is equal to 10. We can see that the plates with higher modulus ratios E_θ/E_r will have higher natural frequencies. The natural frequencies increase quickly when the modulus ratio E_θ/E_r is greater than eight. The phenomenon can be attributed to the rapid growth of membrane stresses σ_r^0 and σ_θ^0. The effects of the Poisson ratio on natural frequencies are plotted in Figure 6. It is shown that the Poisson ratio has little effect on the natural frequencies at low modulus ratio $E_\theta/E_r = 0{\cdot}25$ in Figure 6(a). Larger effects can be seen when $E_\theta/E_r = 4$ in Figure 6(b), especially the effect on the natural frequencies of the mode (0, 2) are so significant. The imaginary natural frequencies will be obtained when $v_r \leqslant -0{\cdot}24$, which implies that the instability referred to the buckle of rotating disks may occur. The reason is that the disks with the negative Poisson ratio v_r will produce compressive membrane stresses due to the rotational inertia forces.

4. FORCED VIBRATION AND STABILITY

After obtaining the natural frequencies and corresponding vibration modes of the disk, the system consisting of a spinning polar orthotropic disk moving in contact with a stationary mass–spring–dashpot system at the point (r_p, φ_p) is now considered (Figure 7). The mass is assumed to closly follow the transverse displacement of the surface of the disk, that is $z = w_p$, and the spring and dashpot are attached to a fixed support adjacent to the

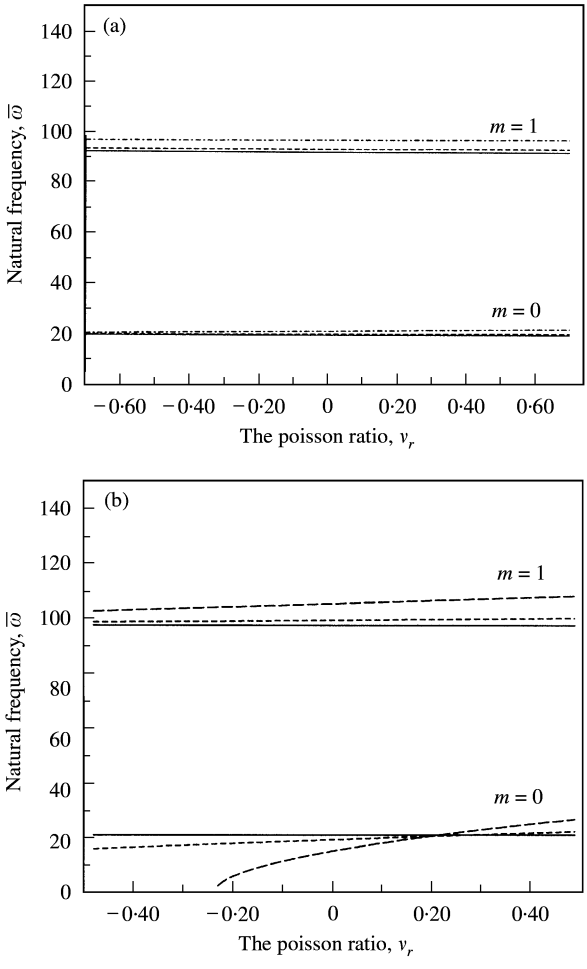

Figure 6. Effects of the Poisson ratios on natural frequencies; (a) $E_\theta/E_r = 0{\cdot}25$: ——, $n = 0$; - - -, $n = 1$; -·-·-·, $n = 2$; (b) $E_\theta/E_r = 4{\cdot}0$ ($a/b = 0{\cdot}5$, $\bar{\Omega} = 10$, $\mu = 0{\cdot}3$): ——, $n = 0$, - - -, $n = 1$; – – –, $n = 2$.

mass. The total force applied to the disk by the system is given by

$$f_p(t) = m_p \frac{\partial^2 z}{\partial t^2} + c_p \frac{\partial z}{\partial t} + s_p z$$

$$= m_p \frac{\partial^2 w_p}{\partial t^2} + c_p \frac{\partial w_p}{\partial t} + s_p w_p, \tag{25}$$

where m_p is the mass, s_p is the spring constant, c_p is the viscous damping coefficient, and w_p is the transverse displacement of the disk. Then the transverse load $q(r, \varphi, t)$ distributed on the disk surface can be expressed as

$$q(r, \varphi, t) = -\frac{1}{r}\delta(\varphi - \varphi_p)\delta(r - r_p) f_p(t)$$

$$= -\frac{1}{r}\delta(\varphi - \varphi_p)\delta(r - r_p)\left(m_p \frac{\partial^2 w}{\partial t^2} + c_p \frac{\partial w}{\partial t} + s_p w\right), \tag{26}$$

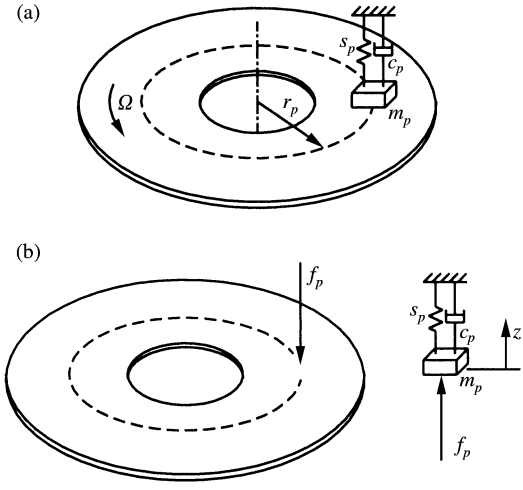

Figure 7. The spinning disk with a stationary concentrated transverse load system.

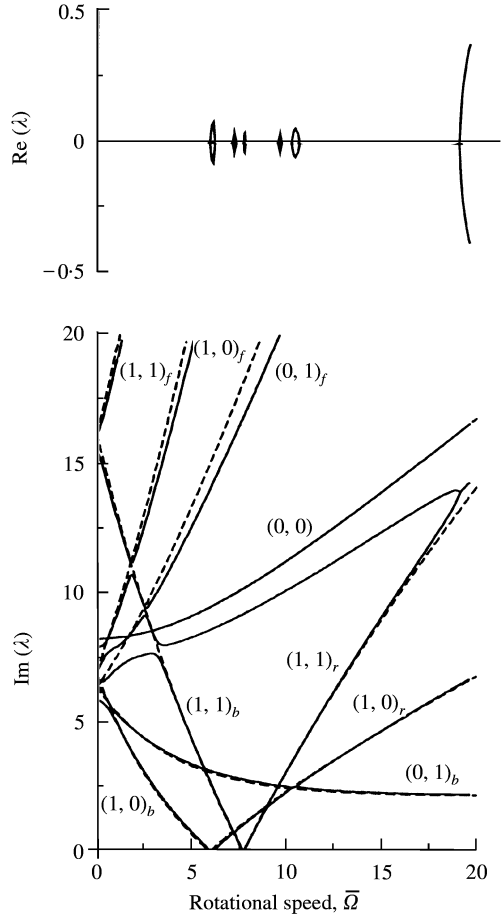

Figure 8. Eigenvalue-rotational speed diagram ($E_0/E_r = 4{\cdot}0$, $v_r = 0{\cdot}3$, $a/b = 0{\cdot}2$, $\mu = 0{\cdot}3$, $\bar{r}_p = 0{\cdot}8$, $\bar{m} = 0{\cdot}1$, $\bar{c} = 0{\cdot}0$, $\bar{s} = 2{\cdot}0$).

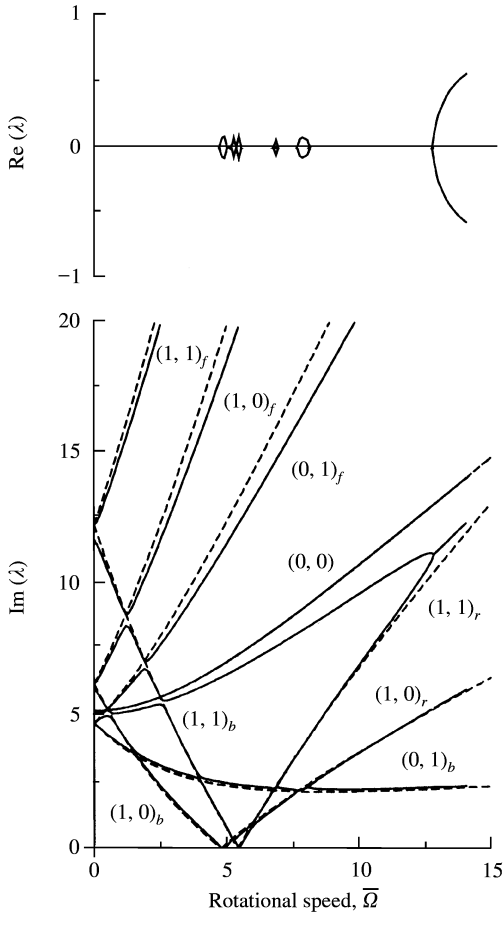

Figure 9. Eigenvalue-rotational speed diagram ($E_\theta/E_r = 1{\cdot}0$, $v_r = 0{\cdot}3$, $a/b = 0{\cdot}2$, $\mu = 0{\cdot}3$, $\bar{r}_p = 0{\cdot}8$, $\bar{m} = 0{\cdot}1$, $\bar{c} = 0{\cdot}0$, $\bar{s} = 2{\cdot}0$).

where $\delta(\,\cdot\,)$ denotes Dirac delta function. The following dimensionless parameters are defined as:

$$\bar{m} = \frac{m_p}{m_0}, \qquad \bar{c} = \frac{c_p}{c_0}, \qquad \bar{s} = \frac{s_p}{s_0}, \qquad m_0 = \rho h \pi b^2, \qquad c_0 = \frac{m_0}{t_0}, \qquad s_0 = \frac{m_0}{t_0^2}. \tag{27}$$

Substituting equations (14), (26) and (27) into equation (11), the equation of motion for the disk can be rewritten in the dimensionless form

$$\frac{\partial^4 \bar{w}}{\partial \bar{r}^4} + \frac{2\alpha}{\bar{r}^2}\frac{\partial^4 \bar{w}}{\partial \bar{r}^2 \partial \varphi^2} + \frac{k^2}{\bar{r}^4}\frac{\partial^4 \bar{w}}{\partial \varphi^4} + \frac{2}{\bar{r}}\frac{\partial^3 \bar{w}}{\partial \bar{r}^3} - \frac{2\alpha}{\bar{r}^3}\frac{\partial^3 \bar{w}}{\partial \bar{r} \partial \varphi^2} - \frac{k^2}{\bar{r}^2}\frac{\partial^2 \bar{w}}{\partial \bar{r}^2} + 2(\alpha + k^2)\frac{1}{\bar{r}^4}\frac{\partial^2 \bar{w}}{\partial \varphi^2}$$

$$+ \frac{k^2}{\bar{r}^3}\frac{\partial \bar{w}}{\partial \bar{r}} - \frac{\bar{\sigma}_r^0}{r}\frac{\partial \bar{w}}{\partial \bar{r}} - \frac{\partial \bar{\sigma}_r^0}{\partial r}\frac{\partial \bar{w}}{\partial \bar{r}} - \bar{\sigma}_r^0\frac{\partial^2 \bar{w}}{\partial \bar{r}^2} - \frac{\bar{\sigma}_\theta^0}{\bar{r}^2}\frac{\partial^2 \bar{w}}{\partial \varphi^2} + \bar{\Omega}^2\frac{\partial^2 \bar{w}}{\partial^2 \varphi} + 2\bar{\Omega}\frac{\partial^2 \bar{w}}{\partial \bar{t} \partial \varphi} + \frac{\partial^2 \bar{w}}{\partial \bar{t}^2}$$

$$= -\frac{\pi}{\bar{r}_p}\delta(\bar{r} - \bar{r}_p)\delta(\varphi - \varphi_p)\left(\bar{m}\frac{\partial^2 \bar{w}}{\partial \bar{t}^2} + \bar{c}\frac{\partial \bar{w}}{\partial \bar{t}} + sw\right). \tag{28}$$

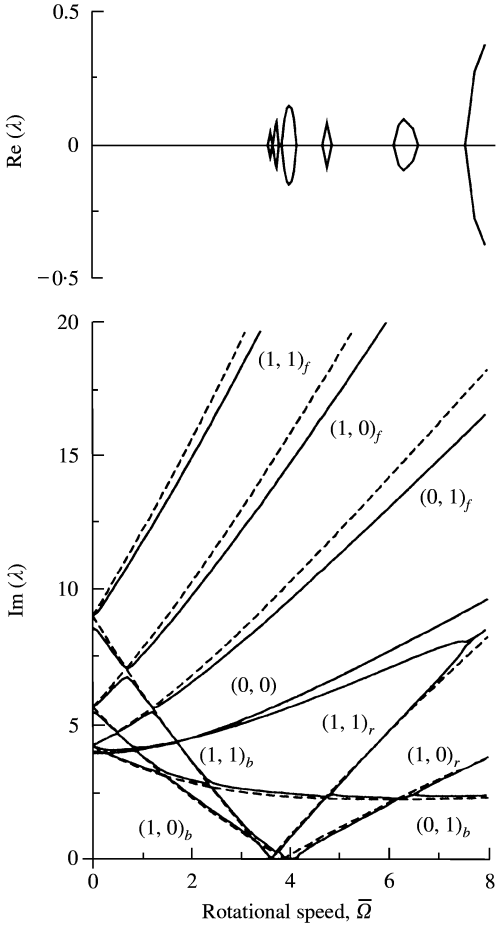

Figure 10. Eigenvalue-rotational speed diagram ($E_\theta/E_r = 0{\cdot}25$, $v_r = 0{\cdot}3$, $a/b = 0{\cdot}2$, $\mu = 0{\cdot}3$, $\bar{r}_p = 0{\cdot}8$, $\bar{m} = 0{\cdot}1$, $\bar{c} = 0{\cdot}0$, $\bar{s} = 2{\cdot}0$).

To solve equation (28), the deflection $\bar{w}$ of the forced vibration can be expressed in an eigenfunction expansion form as

$$\bar{w}(\bar{r}, \theta, \bar{t}) = \sum_{m=0}^{\infty} \sum_{n=0}^{\infty} T_{mn}(\bar{t}) \sin(n\theta - \psi_{mn}) \bar{Y}_{mn}(\bar{r}), \tag{29}$$

where the eigenfunctions $\bar{Y}_{mn}(\bar{r})$ can be obtained from the analysis of free vibration and are orthogonal to each other with respect to different eigenmodes. On space-fixed frame (r, φ, t), substituting equation (10) into equation (29), we obtain

$$\bar{w}(\bar{r}, \varphi, \bar{t}) = \sum_{m=0}^{\infty} \sum_{n=0}^{\infty} [A_{mn}(\bar{t}) \cos n\varphi + B_{mn}(\bar{t}) \sin n\varphi] \bar{Y}_{mn}(\bar{r}), \tag{30}$$

where

$$A_{mn}(\bar{t}) = T_{mn}(\bar{t}) \sin(-n\Omega\bar{t} - \psi_{mn}) \text{ and } B_{mn}(\bar{t}) = T_{mn}(\bar{t}) \cos(-n\Omega\bar{t} - \psi_{mn}).$$

The Galerkin approximation method is used to solve the governing differential equation (28). Substituting equation (30) with finite approximation terms into equation (28),

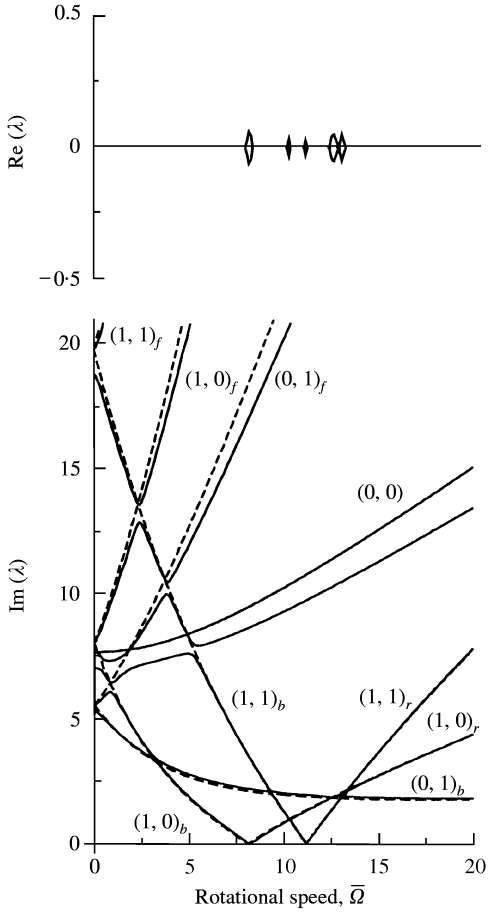

Figure 11. Eigenvalue-rotational speed diagram ($E_\theta/E_r = 4{\cdot}0$, $v_r = 0{\cdot}0$, $a/b = 0{\cdot}2$, $\mu = 0{\cdot}3$, $\bar{r}_p = 0{\cdot}8$, $\bar{m} = 0{\cdot}1$, $\bar{c} = 0{\cdot}0$, $\bar{s} = 2{\cdot}0$).

multiplying by $\bar{r}\bar{Y}_{ij}(\bar{r})(\cos \mathrm{j}\varphi + \sin \mathrm{j}\varphi)$, and then performing integration from 0 to 2π in φ and from ζ to 1 in $\bar{r}$, a system of equations of $A_{ij}(t)$ and $B_{ij}(t)$ can be obtained. The orthogonality of the eigenfunctions of free vibration of a disk is used in the integration procedure. The differential equations in terms of $A_{ij}(t)$ and $B_{ij}(t)$ are expressed as

$$\frac{\mathrm{d}^2 A_{ij}}{\mathrm{d}t^2} + 2n\bar{\Omega}\frac{\mathrm{d}B_{ij}}{\mathrm{d}\bar{t}} + (\bar{\omega}_{ij}^2 - n^2\bar{\Omega}^2)A_{ij} + \sum_{m=0}^{M}\sum_{n=0}^{N}\left[\left(\bar{m}\frac{\mathrm{d}^2 A_{mn}}{\mathrm{d}t^2} + \bar{c}\frac{\mathrm{d}A_{mn}}{\mathrm{d}\bar{t}} + \bar{s}A_{mn}\right)\bar{Y}_{mn}(\bar{r}_p)\,\bar{Y}_{ij}(\bar{r}_p)\right] = 0$$

$$(i = 0, 1, 2, \ldots, M,\ j = 0, 1, 2, \ldots, N). \tag{31}$$

$$\frac{\mathrm{d}^2 B_{ij}}{\mathrm{d}\bar{t}^2} - 2n\bar{\Omega}\frac{\mathrm{d}A_{ij}}{\mathrm{d}\bar{t}} + (\bar{\omega}_{ij}^2 - n^2\bar{\Omega}^2)B_{ij} = 0, \quad (i = 0, 1, 2, \ldots, M,\ j = 0, 1, 2, \ldots, N). \tag{32}$$

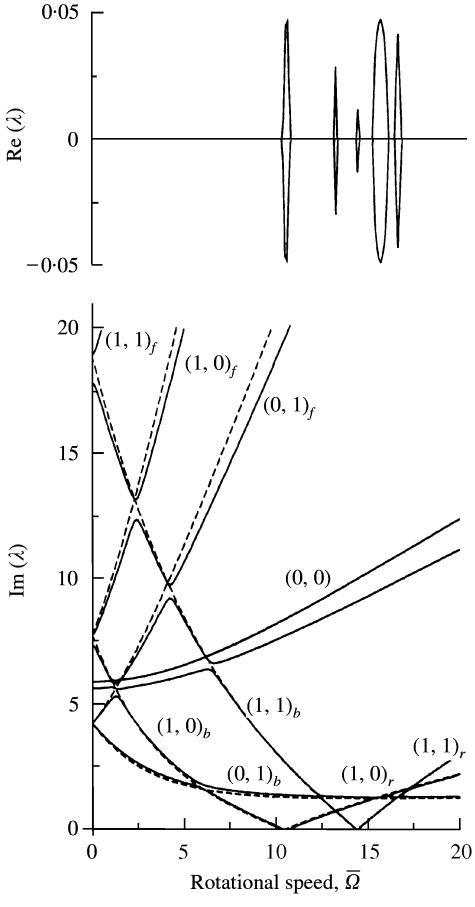

Figure 12. Eigenvalue-rotational speed diagram ($E_\theta/E_r = 4{\cdot}0$, $v_r = -0{\cdot}3$, $a/b = 0{\cdot}2$, $\mu = 0{\cdot}3$, $\bar{r}_p = 0{\cdot}8$, $\bar{m} = 0{\cdot}1$, $\bar{c} = 0{\cdot}0$, $\bar{s} = 2{\cdot}0$).

Equations (31) and (32) form a set of coupled linear ordinary differential equations depending on time. The solution can be assumed as

$$\begin{Bmatrix} \dfrac{\mathrm{d}A_{ij}(\bar{t})}{\mathrm{d}\bar{t}} \\ A_{ij}(\bar{t}) \\ \dfrac{\mathrm{d}B_{ij}(\bar{t})}{\mathrm{d}\bar{t}} \\ B_{ij}(\bar{t}) \end{Bmatrix} = \begin{Bmatrix} \eta_{1ij} \\ \eta_{2ij} \\ \eta_{3ij} \\ \eta_{4ij} \end{Bmatrix} \mathrm{e}^{\lambda\bar{t}} \quad (i = 0, 1, 2, \ldots, M;\ j = 0, 1, 2, \ldots, N), \tag{33}$$

where $\{\eta_{ij}\} = \{\eta_{1ij}\,\eta_{2ij}\,\eta_{3ij}\,\eta_{4ij}\}^{\mathrm{T}}$ is a complex vector and λ is a complex number.

Substituting equation (33) into equations (31) and (32), we can obtain the eigenequations as follows:

$$\lambda\eta_{1ij} + 2n\bar{\Omega}\eta_{3ij} + (\bar{\omega}_{ij} - n^2\bar{\Omega}^2)\eta_{2ij} + \sum_{m=0}^{M}\sum_{n=0}^{N} (\bar{m}\lambda\eta_{1mn} + \bar{c}\eta_{1mn} + \bar{s}\eta_{2mn})\,\bar{Y}_{mn}(\bar{r}_p)\,\bar{Y}_{ij}(\bar{r}_p) = 0$$
$$(i = 0, 1, 2, \ldots, M;\ j = 0, 1, 2, \ldots, N), \tag{34}$$

$$\lambda\eta_{3ij} - 2n\bar{\Omega}\eta_{1ij} + (\bar{\omega}_{ij} - n^2\bar{\Omega}^2)\eta_{4ij} = 0 \quad (i = 0, 1, 2, \ldots, M;\ j = 0, 1, 2, \ldots, N). \tag{35}$$

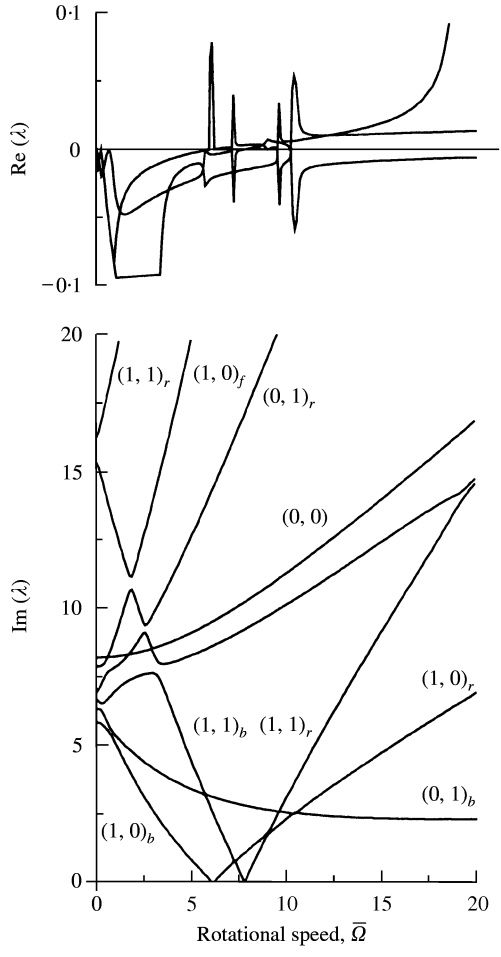

Figure 13. Eigenvalue-rotational speed diagram ($E_\theta/E_r = 4{\cdot}0$, $v_r = 0{\cdot}3$, $a/b = 0{\cdot}2$, $\mu = 0{\cdot}3$, $\bar{r}_p = 0{\cdot}8$, $\bar{m} = 0{\cdot}1$, $\bar{c} = 0{\cdot}1$, $\bar{s} = 2{\cdot}0$).

Then, the eigenvalues of the system can be determined by general numerical methods.

The vibration problems of a spinning polar orthotropic disk subjected to a concentrated transverse load system can be solved and the stability of system will be discussed. Cases of undamped systems ($\bar{c} = 0$) are considered in Figures 8–12; the effects of modulus ratios and the Poisson ratios on the stability are mainly considered. The four lowest modes of eigenvalues are calculated. The plots of eigenvalues versus the rotational speed with different modulus ratios, $E_\theta/E_r = 4{\cdot}0$, $1{\cdot}0$ and $0{\cdot}25$ are shown in Figures 8–10. Since the eigenvalues are complex numbers, the results have been separately plotted in real and imaginary parts of eigenvalues. In these figures, the dashed lines have been added to present the corresponding free vibration case. It can be seen that higher modulus ratios will raise the vibration frequencies (imaginary parts of eigenvalues) and defer the emergence of the critical rotating speed. It indicates that the performance of the whole system will be improved by using the higher modulus ratio orthotropic material of the disk. This is because the higher vibration frequencies of specific modes imply faster travelling wave speeds, thus it is difficult to be caught up with by the rotating speed of the disk to reach the critical speed.

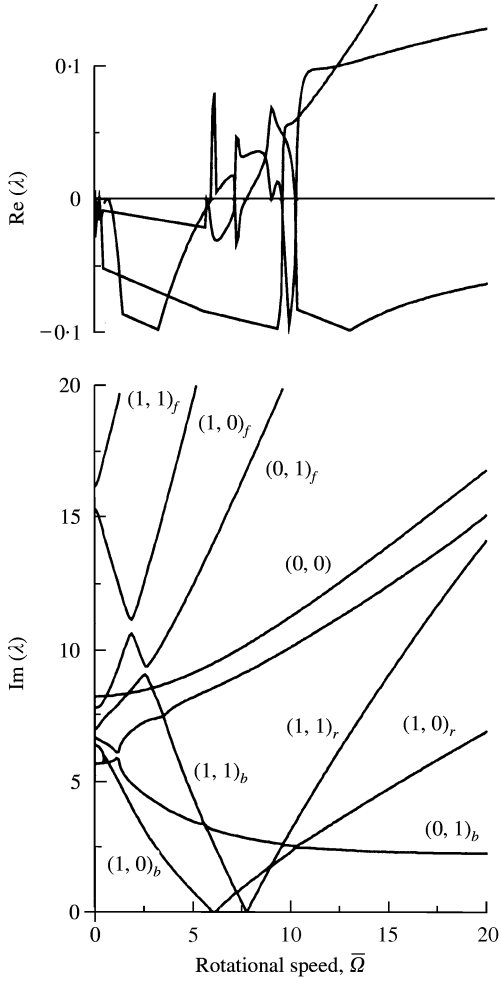

Figure 14. Eigenvalue-rotational speed diagram ($E_\theta/E_r = 4{\cdot}0$, $v_r = 0{\cdot}3$, $a/b = 0{\cdot}2$, $\mu = 0{\cdot}3$, $\bar{r}_p = 0{\cdot}8$, $\bar{m} = 0{\cdot}1$, $\bar{c} = 1{\cdot}0$, $\bar{s} = 2{\cdot}0$).

Similar cases are considered for different Poisson ratios in Figures 11 and 12 respectively. The Poisson ratios $v_r = 0{\cdot}0$ and $-0{\cdot}3$ are chosen. The relations between the eigenvalues and rotational speed are presented again. We can see that the critical speeds increase and the occurrence of the instability region is postponed because of the effect of the negative Poisson ratio.

Figures 13 and 14 present the results of damped systems with the modulus ratio $E_\theta/E_r = 4{\cdot}0$, and dimensionless damping factors are chosen to be $0{\cdot}1$ and $1{\cdot}0$ respectively. The results show that the load damping will reduce vibrations (corresponding to negative real parts of eigenvalues) for some modes. Comparing with Figure 8, we can see that the unstable speed is higher due to the existence of the load damping for some modes. But for some other modes, the load damping will make the system more unstable and instability regions will become continuous. Also, it is seen that a larger load damping will cause a more serious unstability of the system. These results are similar to those of an isotropic disk presented by Iwan and Moeller [3].

5. CONCLUSIONS

In this paper, the vibration and stability of a spinning polar orthotropic disk with a concentrated transverse load system are studied. The free vibration of the spinning polar orthotropic disk is demonstrated first, and the eigenfunctions obtained from the free vibrations are adopted to solve the vibration problems of a rotating disk in contact with a mass–spring–dashpot system. From the numerical calculations, the main results can be summarized as follows.

1. Spinning disks with higher modulus ratios have higher natural frequencies.
2. Effects of the Poisson ratio on natural frequencies of a spinning disk are not significant at lower modulus ratios. But the effects are obvious when the modulus ratios are high. For the mode (0, 2), the negative Poisson ratio may produce large membrane stress and the buckling phenomenon of the disk may occur.
3. In the forced vibration, the higher modulus ratio E_θ/E_r will raise vibration frequencies and critical revolution speeds. Similar results are found for the effect of the Poisson ratio, which does not change the vibration frequencies apparently, but raises critical revolution speeds and puts off regions of the instability as well.

REFERENCES

1. W. EVERSMAN and R. O. DODSON 1969 *American Institute of Aeronautics and Astronautics Journal* **7**, 2010–2012. Free Vibrations of a centrally clamped spinning circular disk.
2. S. BARASCH and Y. CHEN 1972 *American Society of Mechanical Engineers Journal of Applied Mechanics* **39**, 1143–1144. On the vibration of a rotating disk.
3. W. D. IWAN and T. L. MOELLER 1976 *American Society of Mechanical Engineers Journal of Applied Mechanics* **43**, 485–490. The stability of a spinning elastic disk with a transverse load system.
4. K. ONO, J. S. CHEN and D. B. BOGY 1991 *American Society of Mechanical Engineers Journal of Applied Mechanics* **58**, 1005–1014. Stability analysis for the head–disk interface in a flexible disk drive.
5. J. S. CHEN and D. B. BOGY 1992 *American Society of Mechanical Engineers Journal of Applied Mechanics* **58**, S230–S235. Effects of load parameters on the natural frequencies and stability of a flexible spinning disk with a stationary load system.
6. J. S. CHEN and D. B. BOGY 1992 *American Society of Mechanical Engineers Journal of Applied Mechanics* **59**, 390–397. Mathematical structure of modal interactions in a spinning disk-stationary load system.
7. I. A. MINKARAH and W. H. HOPPMANN 1964 *The Journal of the Acoustical Society of America* **36**, 470–475. Flexural vibrations of cylindrically aeolotropic circular plates.
8. F. GINESU, B. PICASSO and P. PRIOLO 1979 *Journal of Sound and Vibration* **65**, 97–105. Vibration analysis of polar orthotropic annular discs.
9. Y. NARIA 1984 *Journal of Sound and Vibration* **92**, 33–38. Natural frequencies of completely free annular and circular plates having polar orthotropy.
10. F. C. MBAKOGU and M. N. PAVLOVIC 1998 *Applied Acoustic* **54**, 207–228. Closed-form fundmental-frequency estimates for polar orthotropic circular plates.
11. U. S. GUPTA and A. H. ANSARI 1998 *Journal of Sound and Vibration* **213**, 429–445. Free vibration of polar orthotropic circular plates of variable thickness with elastically restrained edge.
12. U. S. GUPTA and A. H. ANSARI 1998 *Journal of Sound and Vibration* **215**, 231–250. Asymmetric vibrations and elastic stability of polar orthotropic circular plates of linearly varying profile.
13. C. PISTONESI and P. A. A. LAURA 1999 *Journal of Sound and Vibration* **228**, 712–716. Forced vibrations of a clamped, circular plate of rectangular orthotropy.
14. R. H. GUTIÉRREZ and P. A. A. LAURA 2000 *Journal of Sound and Vibration* **231**, 1175–1178. Transverse vibrations of a circular plate polar anisotropy with a concentric circular support.
15. S. G. LEKHNITSKII 1968 *Anisotropic Plates*. New York: Gordon and Breach Science Publisher.
16. D. S. LIANG 1997 Vibration and stability of rotating polar orthotropic annular plates subjected to transverse loads (in Chinese). *Master's Thesis, National Cheng Kung University, Taiwan.*